A Digitally Controlled 125 kVdc, 30kW Power Supply with an LCC Resonant Converter Working at Variable DC-link Voltage: Full Scale Prototype Test Results

S. Gavin[1], M. Carpita[1], P. Ecoeur[1], H-P. Biner[2], M. Paolone[3], E. Talon Louokdom[4]

[1]*HES-SO, University of Applied Sciences of Western Switzerland, Yverdon-les-Bains, Switzerland*
[2]*HES-SO, University of Applied Sciences of Western Switzerland, Sion, Switzerland*
[3]*EPFL, Swiss Federal Institute of Technology, Lausanne, Switzerland*
[4]*University of Yaoundé 1, Yaoundé, Cameroon*

Keywords: Resonant converter, high voltage, digital control, dynamic modelling.

Abstract

In this paper, a high output voltage power converter working at variable input DC-link voltage is presented. The variable DC link voltage opens to very interesting solution at system level. However, those solutions will be the subject of futures papers. Only the main power converter structure is presented here. After an evaluation of the most promising converter topologies for the required high voltage and power, eventually an LCC resonant converter with phase shift control has been chosen. The resonant converter is followed by a double secondary high frequency transformer with a two diode voltage doublers. The system has been fully analysed from the theoretical point of view, designed, built and tested. The control system has been fully digital implemented making use of a TI DSP microcontroller, TMS320X28335.

1 Introduction

During the topology choice phase of the DC/DC high voltage converter presented in this paper, several solutions to obtain the required high voltage capability have been evaluated. Starting from the key hypothesis of using a resonant inverter, in order to obtain a high switching frequency at a reasonable loss level, various solutions for the transformer and rectifier stage have been considered. Among the others, a number of multi-stage Cockcroft-Walton solutions have been evaluated [1]-[11]. However, mainly due to the increased system complexity and the relatively low dynamics of this kind of topologies, the decision of adopting a simple high frequency transformer and diode voltage doublers configuration has been taken. The chosen solution is based on the LCC resonant inverter structure, followed by a two stage transformer-rectifier, as shown in figure 1.

This topology has several advantages:

- It can incorporate the parasitic elements of the transformer in the circuit operation.
- It has a small-size blocking capacitor connected in series with the high-voltage transformer.
- It can guarantee the soft-switching on a wide operation range.
- It allow for a voltage gain factor up to (theoretically) 2pu (base: DC link voltage) of the transformer input voltage at the resonant frequency.
- Operation with no reactive energy returned to the input voltage source can be achieved with Phase-Shifted PWM control, even with considerable variations in the output voltage and load. High efficiency can thus be obtained in such conditions.
- The resonant elements voltages and currents can be designed at reasonable values for the required power, input and output voltages (see section 2).
- It allows a dynamic response faster than Cockcroft-Walton based solutions.

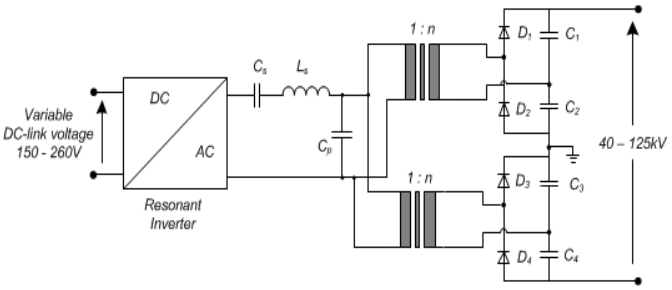

figure 1: High voltage power supply schematic.

2 Steady state theoretical analysis

For the design of the power converter, a theoretical model is required. For this job, the steady-state sinusoidal model proposed in [12] has been used. This model gives a relatively simple analytical method for the analysis of parallel and series-parallel converters with capacitive output filter, to be used in the design procedure for this class of converters.

The basic idea proposed in [12] is to make a theoretical steady-state analysis at the fundamental resonant frequency. This allows obtaining the steady-state equations linking the fundamental harmonic of the various quantities (currents and voltages) of the converter. Those equations have been used in [13], where an optimization strategy, based on a genetic

algorithm approach, has been proposed to find the optimal set of switching frequency and resonant elements.

In this paper a simplified approach is proposed. The design starting hypotheses, obtained from preliminary simulations and feasibility considerations are:

- The transformer voltage ratio has to be between 1:80 and 1:140 for feasibility reasons.
- The magnitude of the ratio between parallel C_p and series C_s capacitors $\alpha_{hyp} = C_p/C_s \approx 0.3$.
- The value of the capacitance C_p should be larger than the transformer parasitic capacitance reported on the primary side, $C_p > C_\sigma \cdot n^2$
- The nominal switching frequency has been chosen as f_s=50 kHz.

The equations presented in [12], [13] have been used to optimize the LCC converter. Even though these equations were written for an LCC converter with simple wave rectifier, we considered they were accurate enough for our circuit containing two parallel transformers with a voltage double rectifier (figure 1), by simply assuming that the transformation ratio were four times higher. This hypothesis has also been verified by simulation.

The converter has then been designed with the following simplified iterative approach.

- The starting operating point is made of the minimum DC-link voltage V_{dc_min}, the maximum power and the nominal switching frequency: V_{dc_min} = 150 V; V_{out} = 120 kV; P_{max}@250 mA, f_s = 50 kHz.
- By imposing the smallest transformation ratio n_{min} the minimum parallel capacity C_{pmin} has been evaluated: n_{min} = 80 which allow obtaining C_{pmin}= 1.6µF.
- A value of Cp compatible with commercially available high voltage, high current, high frequency capacitors has then been chosen, for example Cp= 2.2µF as from High Energy Corp CHN0220M250.
- The capacitance C_s is derived to respect the coefficient α_{th}. $C_s = C_p/\alpha_{hyp} \cong 7.33\mu F$.
- Similarly, a value of existing capacity Cs = 6.2µF(CHN0620M250 High Energy Corp.) has been chosen.
- The actual coefficient α is equal to 0.355, which is a value in the acceptable range.
- From preliminary simulations of the whole LCC converter making use of the values listed above, an IGBT power module Mitsubishi CM600DU-12NFH has been chosen and the efficiency η has been evaluated. Loss coefficients are extracted from the data sheet of the power module.
- figure 2 shows the efficiency as a function of the transformer ratio. The maximum yield is around 1:110 and 1:120. Eventually, the transformation ratio has been chosen 1:110 for each transformer.

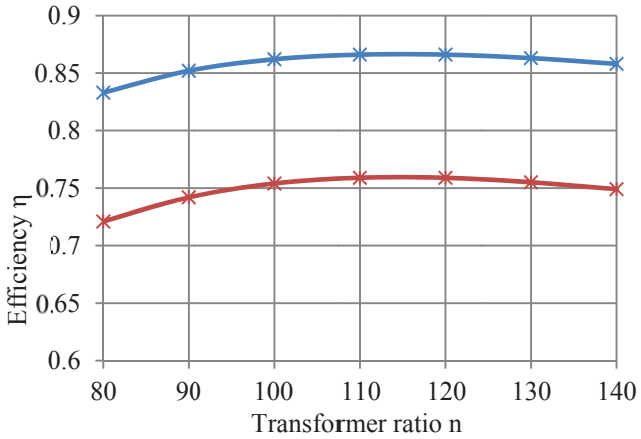

figure 2: Efficiency as a function of the transformer ratio. 120kV/30kW - Vin = 150V (blue) Vin = 200V (red)

Once the transformation ratio chosen, the value of the series inductance can be evaluated. In our case is Ls = 4.65µH.

The main parameters of the LCC converter are summarized in Table 1.

Parameter	Ls	Cs	Cp	n
Value	4.65 µH	6.2 µF	2.2 µF	110

Table 1: Main converter parameters.

3 Dynamic modeling

Let us consider the equivalent circuit shown in figure 3. The capacitors C_{o1}', C_{o2}' and the resistor R_o' are referred to the transformer primary side, $C_{o1}' = C_{o2}' = C_o' = C_o \cdot 2 \cdot n^2$, $R_o' = R_o/(4 \cdot n^2)$.

The equation set used in section 2 is not useful for modeling the dynamic behavior of the power converter, because it is derived from a steady-state approach. A different approach has then been chosen, based on the well-known Generalized Averaging Method proposed in [14]. The same approach for the LCC configuration has been also proposed in [6] and [16].

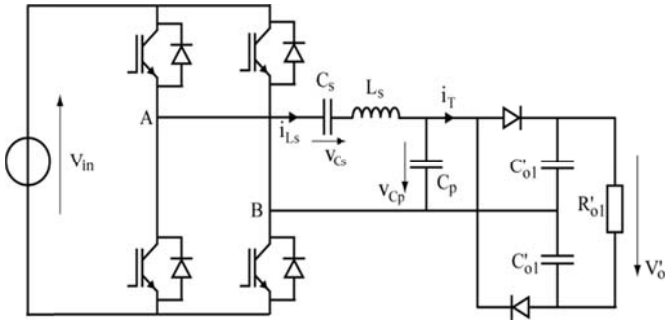

figure 3: LCC converter with voltage doubler

The equations have been written by considering we are using a special kind of phase-shift PWM technique of the converter, the so-called Dual Control as proposed in [15].

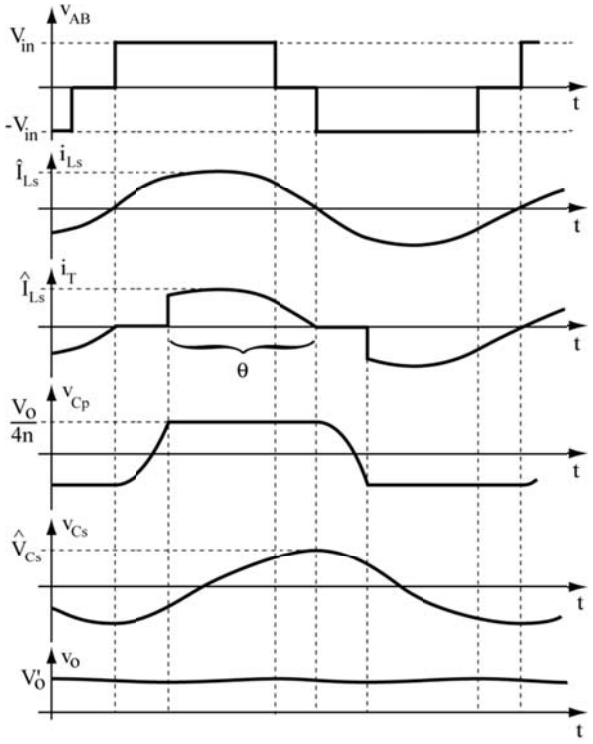

figure 4: Behaviour of the mains variables of the LCC control with Dual Control

This strategy allows reducing the commutation losses, because one of the legs commutates always at zero current. The behavior of the mains variables is represented in figure 4.

The state variables of this converter are the series inductance current i_{Ls}, the series capacitor voltage v_{cs}, and the (referred to primary) output voltage V_o' [6], [16]. The voltage on the parallel capacitor is not a state variable, and it must be expressed as a function of inductance current and the output voltage V_o' [6], [16]. From the equivalent circuit (figure 3), we can write the following differential equations:

$$\frac{di_{Ls}(t)}{dt} = \frac{V_{AB}(t)}{L_s} - \frac{V_{Cs}(t)}{L_s} - \frac{V_{Cp}(t)}{L_s} \quad (1)$$

$$\frac{dV_{Cs}(t)}{dt} = \frac{i_{Ls}(t)}{C_s} \quad (2)$$

$$abs\big(i_T(t)\big) = C_{0'}\frac{dV_o'(t)}{dt} + 2\frac{V_o'}{R_o'} \quad (3)$$

After performing the generalized averaging approach developments on these equations, we obtain the generalized averaging equations as following.

$$\frac{d\langle I_{Ls}\rangle_1}{dt} = -j\omega_s\langle I_{Ls}\rangle_1 + \frac{1}{L_s}\big(-\langle V_{Cs}\rangle_1 - \langle V_{Cp}\rangle_1 + \langle V_{AB}\rangle_1\big) \quad (4)$$

$$\frac{d\langle V_{Cs}\rangle_1}{dt} = -j\omega_s\langle V_{Cs}\rangle_1 + \frac{1}{C_s}\langle I_{Ls}\rangle_1 \quad (5)$$

$$\frac{d\langle V_o'\rangle_0}{dt} = \frac{1}{C_o'}\left(\langle abs(I_T)\rangle_0 - \frac{2.\langle V_o'\rangle_0}{R_o'}\right) \quad (6)$$

Then, the new states variables are: $\langle i_{Ls}\rangle_1$, $\langle V_{Cs}\rangle_1$ and $\langle V_o'\rangle_0$. However, these variables are complex numbers. They can be rewritten by separating the real parts and imaginary parts.
So, $\langle I_{Ls}\rangle_1 = I_{Ld} + I_{Lq}$; $\langle V_o'\rangle_0 = V_o$' $\langle V_{Cs}\rangle_1 = V_{Cd} + V_{Cq}$; $\langle V_{Cp}\rangle_1 = V_{Cpd} + V_{Cpq}$.
Then the equations above can be rewritten as:

$$\frac{dI_{Ld}}{dt} = \omega_s \cdot I_{Lq} - \frac{V_{cd}}{L_s} - \frac{V_{Cpd}}{L_s} + \frac{V_{in}}{\pi \cdot L_s}\sin(\pi D) \quad (7)$$

$$\frac{dI_{Lq}}{dt} = -\omega_s \cdot I_{Ld} - \frac{V_{cq}}{L_s} - \frac{V_{Cpq}}{L_s} + \frac{V_{in}}{\pi \cdot L_s}[\cos(\pi D) - 1] \quad (8)$$

$$\frac{dV_{cd}}{dt} = \omega_s \cdot V_{cq} + \frac{I_{Ld}}{C_s} \quad (9)$$

$$\frac{dV_{cq}}{dt} = -\omega_s \cdot V_{cd} + \frac{I_{Lq}}{C_s} \quad (10)$$

$$\frac{dV_o'}{dt} = \frac{1}{C_o'} \cdot \frac{2 \cdot \sqrt{{I_{Ld}}^2 + {I_{Lq}}^2}}{\pi} \cdot [1 - \cos(\theta)] - \frac{2 \cdot V_o'}{R_o' \cdot C_o'} \quad (11)$$

With

$$\theta = cos^{-1}\left(\frac{\omega_s C_p V_o'}{2 \cdot \sqrt{{I_{Ld}}^2 + {I_{Lq}}^2}} - 1\right) \quad (12)$$

$$V_{Cpd} = \frac{1}{\pi\omega_s C_p}\big[I_{Ld}\delta + I_{Lq}\gamma\big] \quad (13)$$

$$V_{Cpq} = \frac{1}{\pi\omega_s C_p}\big[I_{Lq}\delta - I_{Ld}\gamma\big] \quad (14)$$

Where

$$\gamma = \pi - \theta + 0.5 \cdot \sin(2\theta) \quad (15)$$

$$\delta = \sin(\theta)^2 \quad (16)$$

A few words must be spent on the duty cycle D strategy. The Dual-control is performed by imposing the voltage commutation at each zero crossing of the resonant current. This could induce to think that the direct component of the current should always be zero. However, this component must be taken into account into the dynamic model, because the Dual-control strategy cannot be strictly imposed especially at the beginning of the transient.

4 Simulations

The whole system has been simulated making use of PLECS, power electronics simulation software.

Parameter	Value	Parameter	Value
U_e	150 [V]	C_s	7 [µF]
f_s	60.459 [kHz]	C_p	2.1 [µF]
L_s	4 [µH]	D	0.625 [-]
R_o	680 [kΩ]	C_o	2 [nF]
n (n_2/n_1)	2x110 [-]		

Table 2: Simulation parameters.

To validate the equations (7)-(11), a comparison with the PLECS simulated model has been done. Simulation parameters are shown in Table 2. Those settings are not optimized.

Simulation results are presented in the figure 5. The equations results are shown in red, while the simulated converter results are shown in blue. The calculated average equations values are very close to the simulated average value of instantaneous quantities. However, the equations above have been written with the hypothesis of a fixed resonant frequency, while during actual transient behavior of the converter, the resonance frequency slightly varies.

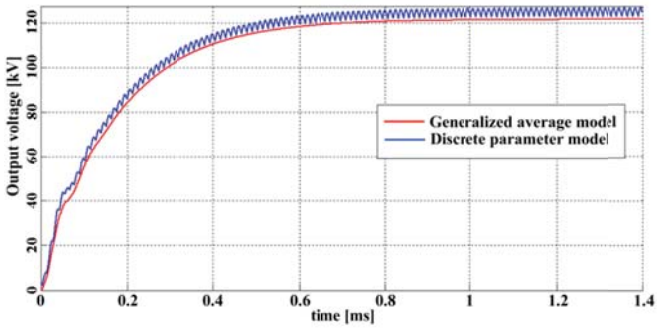

(a)

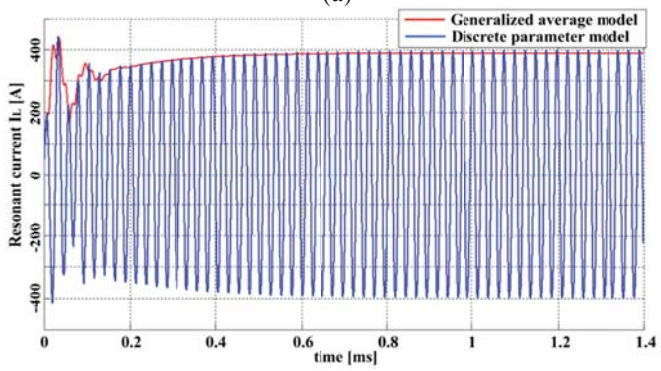

(b)

figure 5: Validation of the generalized averaging equations (a) high voltage transient on the load, (b) resonant current I_L; in red the generalized averaging equations, in blue the discrete parameters model simulation

5 Control strategy

5.1 Transfer function

The generalized equations presented in section 3 are highly non-linear. So, to obtain a useful transfer function, some kind of linearization is mandatory. This is done by firstly set to zero the derivate of equations (7)-(11) to obtain the steady state value of each variable and the relationship with others variables, and secondly by linearizing the equations around the steady state values for small variations of the variables. After the linearization, the classical linearized model of the type given by (17) can be obtained.

$$\begin{cases} \dot{\tilde{x}} = A\tilde{x} + B\tilde{u} \\ \tilde{y} = C\tilde{x} + D\tilde{u} \end{cases} \quad (17)$$

where A, B, C and D are states matrices that describe the system, $\tilde{x}$ is the state vector, $\tilde{u}$ is the input vector, $\tilde{y}$ is the output vector and the symbol ~ means small variations around the steady-state value. In [17], this work has already been done and will then not be repeated here.

5.2 Controller design

The synthesis of the controller has been performed using the pseudo-analog approach [18], [19]. The continuous PI controller parameters have been chosen with the classical gain and phase margin imposition on the Bode diagram and then discretized using standard 'Tustin' bilinear method. As the system is highly dependent on the operating point, some kind of adaptive controller, making use of lookup tables and interpolation has been implemented.

5.3 Modulator and controller implementation on the DSP

The control of the system has been implemented on a Texas Instruments TMS320X28335 "Delfino" microcontroller. This MCU, working at 150MHz clock, has very flexible PWM generation peripherals. In this application the PWM has to work at a variable frequency, synchronized to the resonant current. As already said, a technique based on the zero crossing detection of the resonant current has been implemented. This is done making use of a suitable current transformer and a simple comparator. The PWM modules are then synchronized on the rising edge of the comparator signal.

5.4 Frequency measurement

The actual frequency is measured using a dedicated capture (Cap) unit which consists of a counter running at the CPU frequency. At each rising edge of the comparator signal, the counter is reset and the actual value is stored. This value, which represent the current period expressed in number of CPU cycles, is used by the PWM modules.

5.5 Pulse width modulation signals generation

The resonant converter is a full bridge structure, so two PWM modules are needed, one for each leg. According to the phase shifting technique, each leg is controlled with a 50% duty cycle. The fundamental of the output voltage can be controlled by imposing a suitable phase shift between the two legs. Each PWM module is fully configurable to control both high side and low side power semiconductors including the dead-time generation. Moreover, it can be synchronized either on external events or other PWM modules. In this case, a first modulator (PWM1) will be synchronized on the rising edge of the current sign and a second modulator (PWM2) on the PWM1.

The synchronization is achieved using a straightforward principle: when a sync event occurs, the PWM counter is reset to a known value, which is the required phase lead value as described in [20].

The figure 6 shows a timing diagram of the PWM generation. At each rising edge of the current sign, the Cap module

measures the period and the PWM1 module is then initialized with the period, half-period and phase lead values. If well suited, the phase lead value will compensate the dead-time at each rising edge and eventually allows zero current switching. The PWM2 is synchronized on each period of the PWM1 and so initialized except that the phase lead will be the control variable for the inverter output.

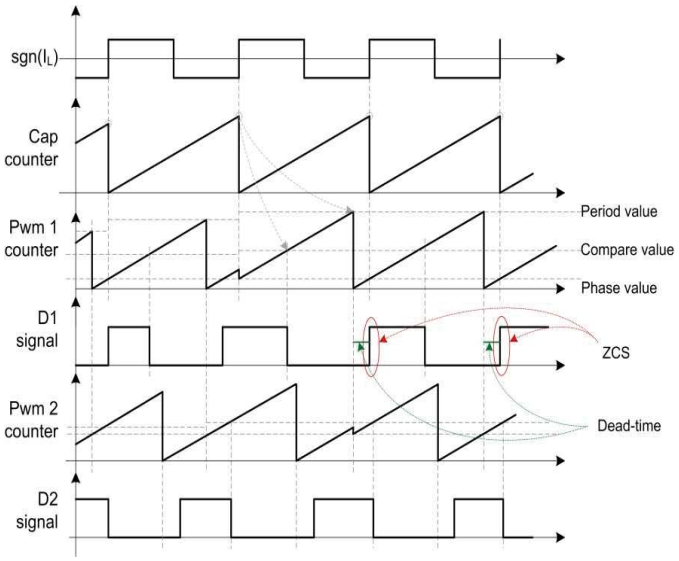

figure 6: Time behavior of the adopted digital phase shifting technique.

6 Preliminary test results

In order to verify the expected behavior of the resonant converter, a prototype has been built.

This prototype consist of a variable DC-link generator able to supply input voltage in the range of 150 – 260 V, a full IGBT bridge of Mitsubishi CM600DU-12NFH, a resonant tank with inductors and capacitors as specified in section 2, two high voltage transformers each with 1:110 turn ratio, rectifiers diodes, capacitors and a resistive dummy load. Each of the four output capacitor has been set to 2nF. Photo of prototype is shown in figure 7.

Experimental tests were done at several operating points. The result of tests shows that the system works as expected. In order to compare experimental results with the simulations done above, an example of output voltage and current shape for the operating point V_{in} = 215 V, R_{load} = 680 kΩ, is shown infigure 8. The output voltage show very low ripple and fast dynamics response (rising time lower than 400µs). The measure output voltage in this case is 122.2 kV with a power of 20 kW.

The shape of the resonant current obtained on the prototype is the same as that obtained in simulations (compare with figure 5 results). The zero crossing detection of resonant current is shown in figure 9. The non-ideal behavior of the voltage clearly shown by the measurements is due to effect of the dead time that has to be imposed to the power component.

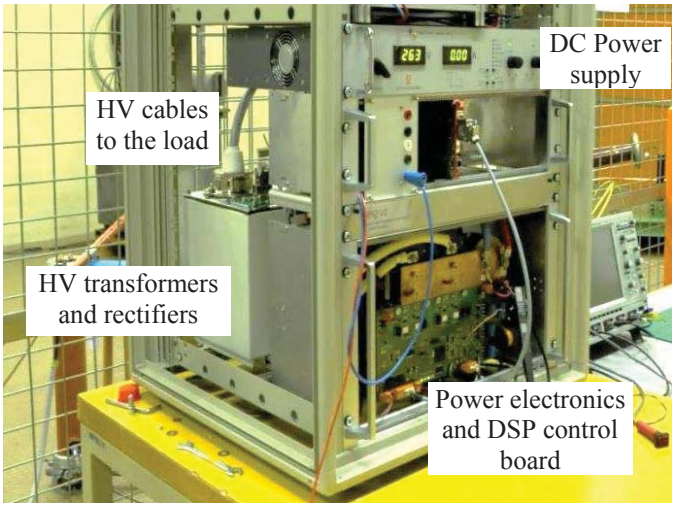

figure 7: Lay-out of the high voltage generator prototype

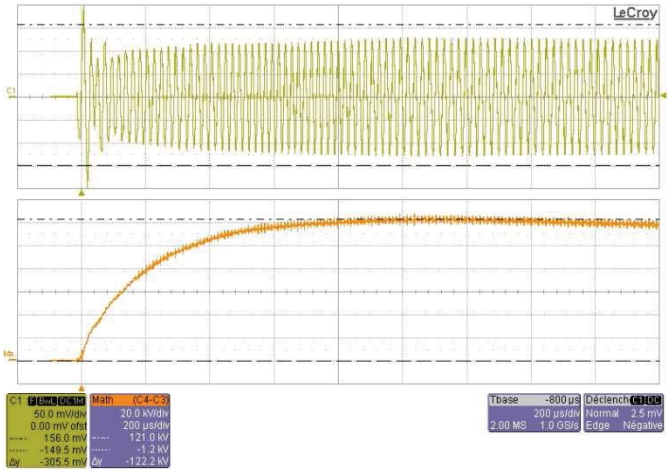

figure 8: Output DC voltage (orange) and resonant current iL (green): Vout = 122.2 kV

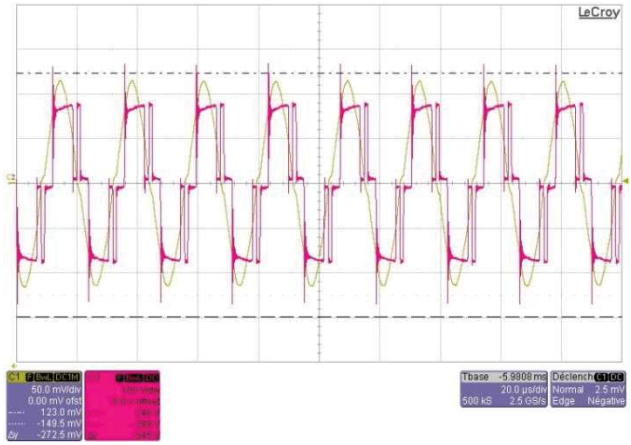

figure 9: Resonant current (yellow) and voltage at the output of the H bridge (pink)

7 Conclusions

In this paper, a high output voltage power converter working at variable input DC-link voltage has been presented. After a careful review of the different topologies presented in literature, an LCC resonant converter topology with phase

shift control has been chosen. The resonant converter is followed by a double secondary high frequency transformer with a two diodes voltage doublers. The system has been fully analyzed from the theoretical point of view, designed, built and tested. A full digital control has been implemented into a TI DSP microcontroller. The experimental results confirm the theoretical and simulation studies.

8 Acknowledgements

The authors gratefully acknowledge T. Camenzind (Swiss Trafo, Josef Betschart AG), for his key contributions to the prototype realisation, to D. Torregrossa, B. Klaiber and K. Schönenberger for their important contribution to the research activity presented in this paper.

This work was supported by the Swiss Federal Commission for Technology and Innovation (CTI).

9 References

[1] L. Malesani, R. Piovan, "Theoretical performance of the capacitor-diode voltage multiplier fed by a current source," *IEEE Transactions on Power Electronics*, **vol.8, no.2**, pp.147,155, (Apr 1993)

[2] J. Sun, X. Ding, M. Nakaoka, H. Takano, "Series resonant ZCS-PFM DC-DC converter with multistage rectified voltage multiplier and dual-mode PFM control scheme for medical-use high-voltage X-ray power generator," *IEE Electric Power Applications Proceedings*, **vol.147, no.6**, pp.527,534, (Nov 2000)

[3] S Liang, Y. Tzou, "DSP control of a resonant switching high-voltage power supply for X-ray generators," *4th IEEE International Conference on Power Electronics and Drive Systems Proceedings*, **vol.2**, pp.522,526, (Oct. 2001)

[4] J.A. Martin-Ramos, J. Diaz, A.M. Pernia, J.M. Lopera, F. Nuno, "Dynamic and Steady-State Models for the PRC-LCC Resonant Topology With a Capacitor as Output Filter," *IEEE Transactions on Industrial Electronics*, **vol.54, no.4**, pp.2262,2275, (Aug. 2007).

[5] T. Melaa, A.K. Ådnanes, K. Öye, T.F. Nestli, R. Nilsen, P. Ranstad, "Evaluation of resonant converters for increased soft switching range," *European Conference on Power Electronics and Applications*, EPE (1997)

[6] F. S. Cavalcante, J. W. Kolar, "Design of a 5kW High Output Voltage Series-Parallel Resonant Converter," *Proceedings of the 34th IEEE Power Electronics Specialists Conference*, **Vol. 4**, pp. 1807-1814, (2003)

[7] S. Iqbal, G.K. Singh, R. Besar, "A Dual-Mode Input Voltage Modulation Control Scheme for Voltage Multiplier Based X-Ray Power Supply," *IEEE Transactions on Power Electronics*, **vol.23, no.2**, pp.1003, (March 2008)

[8] S. Iqbal, R. Besar, C. Venkataseshiah, "A low ripple voltage multiplier for X-ray power supply," *IEEE 2nd International Power and Energy Conference*, pp.1451,1455, (Dec. 2008)

[9] S. Iqbal, R, Besar, C. Venkataseshaiah, "Single/three-phase symmetrical bipolar voltage multipliers for X-ray power supply," *Second International Conference on Electrical Engineering*, pp.1,6, (March 2008)

[10] M. Rentzsch, F. Gleisberg, H.Guldner, F. Benecke, C. Ditmanson, "Closed analytical model of a 20 kV output voltage, 800 W output power series-parallel-resonant converter with Walton Cockroft multiplier," *IEEE Power Electronics Specialists Conference*, pp.1923,1929, (June 2008)

[11] L. Weitao, W. Xu "Development of Electric Control High Power Medical-Use X-Ray Generator," *International Conference on Information Engineering and Computer Science*, pp.1,5, (Dec. 2009)

[12] G. Ivensky, A. Kats, S. Ben-Yaakov, "A novel RC model of capacitive-loaded parallel and series-parallel resonant DC-DC converters," *28th Annual IEEE PESC Record*, **vol.2**, pp.958,964, (Jun 1997)

[13] T. Soeiro, J. Biela, J. Muhlethaler, J. Linnér, P. Ranstad, J.W. Kolar, "Optimal design of resonant converter for Electrostatic Precipitators," *International Power Electronics Conference*, pp.2294,2301, (June 2010)

[14] S.R. Sanders, J.M. Noworolski, X.Z. Liu, G.C. Verghese, "Generalized averaging method for power conversion circuits," *IEEE Transactions on Power Electronics*, **vol.6, no.2**, pp.251,259, (Apr 1991)

[15] P. Ranstad, H-P. Nee, J. Linner, "A novel control strategy applied to the series loaded resonant converter," *European Conference on Power Electronics and Applications*, pp.10, (2005)

[16] J.A. Martin-Ramos, J. Diaz, A.M. Pernia, F. Nuno, J. Sebastian, "Large-signal modelling of the PRC-LCC resonant topology with a capacitor as output filter," *IEEE APEC 2002*, **vol.2**, pp.1120,1126 (2002)

[17] F.S. Cavalcante, J.W. Kolar, "Small-Signal Model of a 5kW High-Output Voltage Capacitive-Loaded Series-Parallel Resonant DC-DC Converter," *IEEE PESC '05*, pp.1271,1277, (June 2005)

[18] M. Carpita, M. Pellerin, J. Herminjard, "Medium Frequency Transformer for Traction Applications making use of Multilevel Converter: Small Scale Prototype Test Results," *International Symposium on Power Electronics, Electrical Drives, Automation and Motion SPEEDAM proceedings*, pp.1095-1100, (2006)

[19] M. Carpita, T. Beltrami, C. Besson, S. Gavin, "Multiphase Active Way Linear Motor: Proof-of-Concept Prototype," *IEEE Transactions on Industrial Electronics*, **vol. 59, n. 5**, (May 2012)

[20] M. Carpita, M. De Vivo, S. Gavin, "A bidirectional DC/DC interleaved converter for supercapacitor applications," *5th European DSP Education and Research Conference proceedings*, pp.149 – 153, (sept. 2012)